2007

# The cohesive element approach to dynamic fragmentation: The question of energy convergence

J F. Monlinari
*Department of Mechanical Engineering, Johns Hopkins University*, molinari@jhu.edu

G Gazonas
*U.S. Army Research Laboratory, Weapons and Materials Research Directorate*

R Raghupathy
*Department of Mechanical Engineering, Johns Hopkins University*

A Rusinek
*LPMM, University of Metz*

F Zhou
*Department of Mechanical Engineering, Johns Hopkins University*

INTERNATIONAL JOURNAL FOR NUMERICAL METHODS IN ENGINEERING
*Int. J. Numer. Meth. Engng* 2007; **69**:484–503
Published online 5 June 2006 in Wiley InterScience (www.interscience.wiley.com). DOI: 10.1002/nme.1777

# The cohesive element approach to dynamic fragmentation: The question of energy convergence

J. F. Molinari[1,*,†], G. Gazonas[2], R. Raghupathy[1], A. Rusinek[3] and F. Zhou[1]

[1]*Department of Mechanical Engineering, Johns Hopkins University, 104 Latrobe Hall, 3400 N. Charles Street, Baltimore, Maryland 21218, U.S.A.*
[2]*U.S. Army Research Laboratory, Weapons and Materials Research Directorate, Attn: AMSRD-ARL-WM-MD; Aberdeen Proving Ground, MD 21005-5066 U.S.A.*
[3]*LPMM, University of Metz, 57000, France*

SUMMARY

The cohesive element approach is getting increasingly popular for simulations in which a large amount of cracking occurs. Naturally, a robust representation of fragmentation mechanics is contingent to an accurate description of dissipative mechanisms in form of cracking and branching. A number of cohesive law models have been proposed over the years and these can be divided into two categories: cohesive laws that are initially rigid and cohesive laws that have an initial elastic slope. This paper focuses on the initially rigid cohesive law, which is shown to successfully capture crack branching mechanisms in simulations. The paper addresses the issue of energy convergence of the finite-element solution for high-loading rate fragmentation problems, within the context of small strain linear elasticity. These results are obtained in an idealized one-dimensional setting, and they provide new insight for determining proper cohesive zone spacing as function of loading rate. The findings provide a useful roadmap for choosing mesh sizes and mesh size distributions in two and three-dimensional fragmentation problems. Remarkably, introducing a slight degree of mesh randomness is shown to improve by up to two orders of magnitude the convergence of the fragmentation problem. Copyright © 2006 John Wiley & Sons, Ltd.

Received 21 July 2005; Accepted 10 April 2006

KEY WORDS: dynamic crack propagation; crack branching; fragmentation; cohesive element; numerical convergence

*Correspondence to: J. F. Molinari, Department of Mechanical Engineering, Johns Hopkins University, 104 Latrobe Hall, 3400 N. Charles Street, Baltimore, Maryland 21218, U.S.A.
†E-mail: molinari@jhu.edu

Contract/grant sponsor: Army Research Office; contract/grant number: 48389-MS
Contract/grant sponsor: Army Research Laboratory; contract/grant number: 2511050005200

## 1. INTRODUCTION

Structures often develop complex fracture and fragmentation patterns during the failure process, and the quest for understanding the pattern and distribution of fragment size has captured the attention and imagination of the scientific community for many decades. Models for predicting fragment size distribution have been applied to understand the physics of hypervelocity impact [1, 2], crash performance, explosive drilling [3], and even the size distribution and clustering of galaxies resulting from the formation of the universe during the big bang [4]. Armor ceramics are another important class of materials that fail on impact due to a fast fragmentation process [5]. It has been observed that the interaction between the penetrator and the fragmented zone ahead of it (often referred to as the comminuted or Mescal zone) is key to penetration performance [6].

Despite this large body of work, our understanding of the physics of fragmentation is still incomplete. The difficulty emanates from the inherent multi-scale nature of the fracture process. In the case of ceramic materials, it is well known that strength, crack initiation, and crack propagation are affected by the presence of flaws at the micrometer scale. Under dynamic loading conditions, cracks will initiate at these flaws, and potentially propagate catastrophically to cause large-scale structural failure. Multiple cracks will initiate at seemingly random locations and material failure will occur through a complex communication process of stress-wave interactions between cracks.

Evidently, due to the space and time-varying nature of the problem, the use of classical fracture mechanics analysis is limited. Recent developments in the field of computational solid mechanics, including large-scale parallel simulations, enable a fresh look at fragmentation mechanics. Novel simulation techniques permit a new insight and an ever-closer agreement between experiments and modelling. An example of such a numerical approach is the cohesive element method. Cohesive elements originate from the concept of cohesive zone, which was first introduced by Dugdale [7] and Barrenblatt [8]. The implementation of a cohesive zone into numerical analysis takes the form of cohesive elements, which explicitly simulate the crack process zone. Many examples of applications that utilize cohesive elements may be found in the literature [9–22].

The cohesive element approach has gained in popularity over the years. This is principally due to its ease of implementation and the clear physical picture that is given by the explicit representation of cracks. Crack branching and fragmentation are often presented in the literature as natural outcomes of the method. Nonetheless, despite the success of the approach several topics of controversy remain. A first item that will be briefly discussed in the paper is the choice of the cohesive law. We have shown in a different work that the shape of the cohesive-law softening curve has little effect on the fragmentation results [20, 23]. This paper illustrates that initially rigid cohesive laws can successfully model the 'side-branching' fracture mechanism [24, 25]. Perhaps a more fundamental issue has to do with convergence of the method. Recently Papoulia *et al.* have provided computational evidence of mesh convergence of the crack path. Convergence was observed for a special category of meshes referred to as pinwheel-based meshes [26]. Crack path convergence will not be addressed in this paper, which will be solely and fully devoted to the evolution of microcrack density as function of mesh size. In the creation of new surfaces, each opening cohesive element dissipates a given amount of energy (e.g. cohesive energy). The total energy dissipated in the cracking problem is therefore clearly related to the crack path and thus mesh convergence. Energy convergence of the finite-element solution has been mainly eluded



DOI: 10.1002/nme

in the literature. It has been generally observed that for a fixed strain rate, finer meshes lead to higher energy dissipation due to more microcracking [17]. To the best of our knowledge, no demonstration of solution convergence has been shown in large-scale fragmentation problems. The issue of energy convergence during the cracking process is of fundamental importance as it clearly affects the physical robustness of the numerical methodology; it is the main purpose of the paper.

Section 2 of the paper briefly describes the finite element methodology, including the cohesive element approach. It also provides background regarding key length scales and time scales associated with cohesive elements. A two-dimensional crack-branching simulation is given to illustrate the approach. Section 3 analyses convergence issues in a simplified one-dimensional setting and implications for the extension to multidimensional finite element simulations.

## 2. FINITE ELEMENT METHODOLOGY, ASSOCIATED LENGTH SCALES AND TIME SCALES

We begin with a brief review of the adopted finite element framework. The context is explicit dynamics, small strain linear elasticity. More details may be found in References [12, 14, 21], or in standard finite element books [27].

### *2.1. Explicit dynamic finite-element analysis*

We discretize a body $B_0$ with line-segment elements in 1D, quadratic triangular elements in 2D (T6), or quadratic tetrahedral elements in 3D (T10). Upon discretization, the principle of virtual work applied to the equations of equilibrium renders:

$$\mathbf{M}\ddot{\varphi} + \mathbf{R}^{\text{int}}(\varphi) = \mathbf{R}^{\text{ext}}(t) \tag{1}$$

where $\mathbf{R}^{\text{ext}}$ and $\mathbf{R}^{\text{int}}$ are the external and internal forces arrays, $\mathbf{M}$ is the mass matrix, and $\boldsymbol{\varphi}$ is the nodal co-ordinates array.

This equation is integrated along the time axis by the second-order accurate explicit scheme. The explicit version of the Newmark scheme is obtained taking the Newmark's parameters to be $\beta = 0$ and $\gamma = \frac{1}{2}$, as

$$\begin{aligned} \varphi_{n+1} &= \varphi_n + \Delta t\,\mathbf{v}_n + \tfrac{1}{2}\Delta t^2 \mathbf{a}_n \\ \mathbf{a}_{n+1} &= \mathbf{M}^{-1}(\mathbf{R}^{\text{ext}}_{n+1} - \mathbf{R}^{\text{int}}_{n+1}) \\ \mathbf{v}_{n+1} &= \mathbf{v}_n + \tfrac{1}{2}\Delta t\,(\mathbf{a}_n + \mathbf{a}_{n+1}) \end{aligned} \tag{2}$$

where $\mathbf{v}$ and $\mathbf{a}$ are the material velocity and acceleration fields. In this scheme, the mass matrix $\mathbf{M}$ is lumped and diagonal.

To guarantee the stability of the time integration, the time step $\Delta t$ must be lower than a critical value, $\Delta t_{\text{stable}}$, which is related to the dilatational (the fastest) wave speed and the (smallest) mesh size. In our simulation, the time step is taken as

$$\Delta t = C\Delta t_{\text{stable}} = C \min_{\text{mesh}} \left( \frac{h_{\text{e}}}{\sqrt{(\lambda + 2\mu)/\rho}} \right) \tag{3}$$



DOI: 10.1002/nme

where $C$ is a time step scale factor ($C<1.0$, an ordinary value is about 0.1), $h_e$ is the dimension of the element, $\lambda$, $\mu$, and $\rho$ are the Lamé coefficients, and the density of the material. The quantity $\sqrt{(\lambda+2\mu)/\rho}$ is the longitudinal wave speed in an unbounded medium. In a 1D problem the interpretation of $h_e$ is straightforward; in multidimensional setting the radius of the in circle or in sphere are taken as the element sizes.

### 2.2. *Cohesive element method*

In the finite element analysis, the specimen is discretized with ordinary continuum elements. The interfaces between two neighbouring elements (line segments in 2D or facets in 3D) are treated as possible sites for cracks; see Figure 1(a) for a 2D schematic. We use the initially rigid cohesive law, Figure 1(b), proposed by Camacho and Ortiz [12] and at a later time by Pandolfi *et al.* [14] in a 3D setting. Using this type of law implies that cohesive elements have to be added on the fly, a scheme sometimes referred to as dynamic insertion [28]. The initial finite-element mesh is free of cohesive elements, and as the dynamic simulation proceeds, cohesive elements are inserted at locations where the stress exceeds a critical value $\sigma_c$. Several methods have been proposed for identifying what constitutes a sensible insertion criterion. A discussion on various methods for dynamically inserting cohesive elements into the finite element mesh is given by Papoulia *et al.* [29]. The two-dimensional results shown in this paper were obtained by using an average of the normal component of the stress tensor to an element edge. For quadratic elements, four Gauss Points contribute to this average. Clearly, the implementation of a dynamic insertion scheme necessitates extensive computational bookkeeping, but this methodology avoids artificially altering the elastic properties of the medium or structure. Indeed, in other cohesive law models, such as the exponential cohesive law [24], the element's initial response amounts to adding a spring in the mesh, and this may substantially change the problem's response.

The initially rigid cohesive model, which is used in the remainder of the paper, is illustrated in Figure 1(b). We have shown in previous work [23] that the shape of the unloading curve does

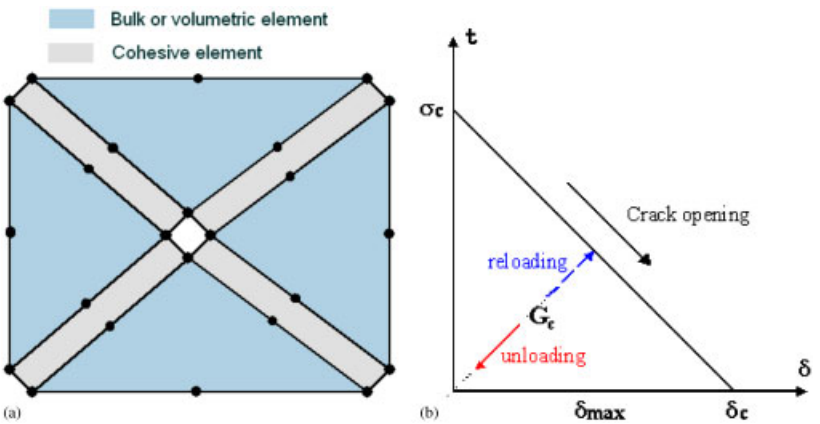


Figure 1. (a) Finite element discretization with triangular bulk/continuum elements (six nodes) and corresponding cohesive elements; and (b) initially rigid, linear-decaying irreversible cohesive law.



DOI: 10.1002/nme

not change significantly the fragmentation results. Therefore, we use a simple irreversible linear decaying cohesive law:

$$\begin{aligned} \frac{t}{\sigma_c} &= 1 - \frac{\delta}{\delta_c} \qquad \text{for } \dot{\delta}>0, \quad \delta = \delta_{\max} \\ \frac{t}{\sigma_c} &= \frac{\delta}{\delta_{\max}} - \frac{\delta}{\delta_c} \quad \text{for } \delta<\delta_{\max} \end{aligned} \tag{4}$$

where $t$ is an effective traction, $\delta$ is an effective displacement, $\sigma_c$ is the maximum cohesive force, and $\delta_c$ is the critical opening distance. Note that a cohesive element resists opening until it is fully damaged ($\delta_{\max} = \delta_c$). The notion of an effective displacement should be further explicated. The original idea developed by Camacho and Ortiz [12] is that the response of a cohesive element should depend on a combination of normal and shear deformations. They defined the effective opening displacement $\delta$ as

$$\delta = \sqrt{\beta^2 \delta_{\mathrm{s}}^2 + \delta_{\mathrm{n}}^2} \tag{5}$$

where $\delta_{\mathrm{n}}$ and $\delta_{\mathrm{s}}$ are the normal and shear opening displacements over the cohesive surface. The parameter $\beta$ assigns different weights to the sliding and normal opening displacements. Similarly, the effective traction $t$ is defined as

$$t = \sqrt{\beta^{-2} |t_{\mathrm{s}}|^2 + t_{\mathrm{n}}^2} \tag{6}$$

where $t_{\mathrm{s}}$ and $t_{\mathrm{n}}$ are the shear and normal tractions. Clearly, a negative $\delta_{\mathrm{n}}$ indicates that contact is occurring. In this paper we enforce a simplistic contact algorithm in which contacting facets are modelled as a perfect junction with no overlap. At contact locations, compressive stress waves travel through the material as if it were undamaged until tensile waves reopen these cohesive elements.

Three material parameters are associated with this choice of cohesive law. The physical meanings of $\sigma_c$ and $\delta_c$ have been described earlier. The third parameter, which is not independent of the other two but is often easier to evaluate, corresponds to the area under the curve of Figure 1(b). It is the fracture energy that is needed to fully open a unit area of crack surface:

$$G_c = 2\Gamma_c = \frac{\sigma_c \delta_c}{2} \tag{7}$$

where $\Gamma_c$ is the surface energy.

Clearly, the success of simulations using cohesive elements resides largely in the proper choice of the material parameters. Additionally, it is contingent to resolving appropriate length scales and time scales associated with the fragmentation process. The next section revisits some key concepts in this regard.

### *2.3. Associated length scales and time scales*

Various length scales and time scales are associated with cohesive elements. They are functions of elastic and fracture material properties. The following convention is adopted: $E$ is the Young's modulus, $\rho$ the mass density, $c$ the wave speed, $\sigma_c$ the critical stress at which the decohesion process begins, $G_c$ the critical energy release rate, $\delta_c$ the critical opening displacement, and $\dot{\varepsilon}$ the loading rate.



DOI: 10.1002/nme

*2.3.1. Cohesive zone concept.* In order to properly capture the physics of dynamically failing material in the vicinity of the crack tip in numerical simulations, it is important that the finite element mesh size be smaller than the cohesive zone length. The number of finite elements needed to model the behaviour at the tip of the crack will be highly dependent upon the constitutive description of the cohesive zone and bulk continuum, and the nature and rapidity of the internal and external loadings.

If the cohesive zone tractions or 'failure stresses' are constant and independent of position along the failure zone, viz, $\sigma_f(\xi) = \sigma_c$, where $\xi$ is the co-ordinate along the cohesive zone, a number of authors [30–32] have shown that the cohesive zone length $\alpha$ can be written as

$$\alpha = \frac{\pi}{8}\left(\frac{K_{\mathrm{I}}}{\sigma_c}\right)^2 = \frac{\pi}{8}\frac{EG_c}{\sigma_c^2(1-\nu^2)} \tag{8}$$

where $K_{\mathrm{I}}$ is the mode-I stress intensity factor. The expression for the cohesive zone length is obtained by solving a boundary value problem using the method of superposition; here, it is assumed that it is permissible to sum the stresses $\sigma_y^0$ in the neighbourhood of the crack tip without a cohesive zone due to loads acting in and on the elastic continuum, with the stresses induced in the solid due to a failure stress distribution $\sigma_y^f$ at the tip of a crack with a cohesive zone [8]. Using the notation in Reference [31], the superposition can be expressed as

$$\sigma_y = \sigma_y^0 + \sigma_y^f \tag{9}$$

where, for example, the $y$-component of stress in a linear elastic medium on $y = 0$, and close to the crack tip, is given by Williams [33] as

$$\sigma_y^0(\xi_1) = \frac{K_{\mathrm{I}} H(\xi_1)}{\sqrt{2\pi\xi_1}} \tag{10}$$

where $H$ is the Heaviside function, and the stresses due to the action of the cohesive zone failure stresses [8, 31] very close to the crack tip are given by

$$\sigma_y^f = \frac{-1}{\pi\sqrt{\xi_1}}\int_0^\alpha \frac{\sigma_f(\xi)\,\mathrm{d}\xi}{\sqrt{\xi}} + \mathrm{HOT} \tag{11}$$

Substitution of Equations (10) and (11) into Equation (9), yields the resultant stress in the linear elastic continuum,

$$\sigma_y = \frac{K_{\mathrm{I}} H(\xi_1)}{\sqrt{2\pi\xi_1}} - \frac{1}{\pi\sqrt{\xi_1}}\int_0^\alpha \frac{\sigma_f(\xi)\,\mathrm{d}\xi}{\sqrt{\xi}} + \mathrm{HOT} \tag{12}$$

Since the higher-order terms in Equation (12) are finite, then $\sigma_y$ will be finite if and only if the first two terms can be equated, viz,

$$K_{\mathrm{I}} = \sqrt{\frac{2}{\pi}}\int_0^\alpha \frac{\sigma_f(\xi)\,\mathrm{d}\xi}{\sqrt{\xi}} \tag{13}$$

By substituting the assumption that $\sigma_f(\xi) = \sigma_c$ into Equation (13) the result given in Equation (8) is readily obtained. In another case, where it is assumed that the failure stress varies linearly



DOI: 10.1002/nme

within the cohesive zone $\sigma_f(\xi) = \sigma_c(1 - \xi/\alpha)$, Palmer and Rice [34] (and also Rice [32]) derive a cohesive zone length, which is $\frac{9}{4}$ times the estimate in Equation (8), i.e.

$$\alpha = \frac{9\pi}{32}\left(\frac{K_{\mathrm{I}}}{\sigma_c}\right)^2 = \frac{9\pi}{32}\frac{EG_c}{\sigma_c^2(1-\nu^2)} \tag{14}$$

Equations (8) and (14) provide *static* estimates for the cohesive zone length. Clearly, a simulation that includes cohesive elements should have elements smaller than this dimension to resolve the fragmentation process. This procedure is now commonly adopted in the literature [24, 35]. Nonetheless, later in this paper, we will question the appropriateness of using this length scale in dynamic fracture and fragmentation simulations.

*2.3.2. Time scale associated with opening of cohesive element.* Once a fine enough finite-element discretization is obtained, the use of cohesive elements results in an additional length scale. This is a consequence of the time associated with the opening of an isolated microcrack [12]. Part of the analysis that follows was developed in Reference [23] and only the essential features are summarized herein.

For argument's sake, we consider a bar made of a linear elastic material. The bar is loaded uniformly in tension up to rupture. The cohesive behaviour follows an initially rigid linear decreasing cohesive law (Figure 1(b)).

The following ordinary differential equation governs the monotonic unloading behaviour in an isolated cohesive element [23]:

$$\sigma_c\left(1 - \frac{\delta_{\mathrm{coh}}}{\delta_c}\right) - \sigma_c = -\rho c\left(\frac{\dot{\delta}_{\mathrm{coh}}}{2} - \dot{\varepsilon}ct\right) \tag{15}$$

where $\delta_{\mathrm{coh}}$ denotes the opening displacement of the cohesive element (initially it is zero). The ordinary differential equation (15) can be simplified by normalizing the variables similarly to Drugan [36]:

$$\overline{\delta}_{\mathrm{coh}} = \frac{\delta_{\mathrm{coh}}}{\delta_c}, \quad \overline{t} = \frac{2\sigma_c t}{\rho c \delta_c} = \frac{t}{t_0}, \quad \overline{\dot{\varepsilon}} = \frac{\dot{\varepsilon}}{\dot{\varepsilon}_0} \tag{16}$$

where the characteristic time $t_0$ [12], to be understood as the 'response' time of the cohesive element, is

$$t_0 = \frac{\rho c \delta_c}{2\sigma_c} = \frac{E}{2\sigma_c}\left(\frac{\delta_c}{c}\right) = \frac{EG_c}{c\sigma_c^2} \tag{17}$$

and $\dot{\varepsilon}_0$, a derivative of the characteristic time scale, is the *characteristic strain-rate* [23]:

$$\dot{\varepsilon}_0 = \frac{\sigma_c/E}{t_0} = \frac{2\sigma_c^2}{\rho^2 c^3 \delta_c} = \frac{2c\sigma_c^2}{E^2\delta_c} = \frac{c\sigma_c^3}{E^2 G_c} \tag{18}$$

Note that this is also an intrinsic material parameter, and determines whether a particular externally applied strain rate is perceived as a low or high strain rate during this dynamic decohesion process. The non-dimensional ordinary differential equation and initial condition are:

$$\overline{\delta}_{\mathrm{coh}} = \frac{\mathrm{d}\overline{\delta}_{\mathrm{coh}}}{\mathrm{d}\overline{t}} - \overline{\dot{\varepsilon}}\overline{t} \tag{19a}$$



DOI: 10.1002/nme

and

$$\overline{\delta}_{\mathrm{coh}}|_{\overline{t}=0} = 0 \tag{19b}$$

This equation is readily solved as

$$\overline{\delta}_{\mathrm{coh}} = \overline{\dot{\varepsilon}}[\exp(\overline{t}) - \overline{t} - 1] \tag{20}$$

Equation (20) describes the dynamics of an isolated decohesion: the evolution of the cohesive crack opening displacement for an isolated crack in an expanding bar. The crack opening displacement is a non-linear, monotonically increasing function of time, controlled by the material properties and the external loading $\dot{\varepsilon}$. Substituting (20) into the cohesive law, the non-dimensional cohesive stress may now be expressed as

$$\overline{\sigma}_{\mathrm{coh}} \equiv \frac{\sigma_{\mathrm{coh}}}{\sigma_c} = 1 - \overline{\dot{\varepsilon}}[\exp(\overline{t}) - \overline{t} - 1] \tag{21}$$

The critical time $\overline{t}_c$ at which the decohering point completely fails can be computed by setting $\overline{\sigma}_{\mathrm{coh}} = 0$ in Equation (21):

$$\overline{\dot{\varepsilon}}[\exp(\overline{t}_c) - \overline{t}_c - 1] = 1 \tag{22}$$

For the purpose of this study, we are interested in the high strain rate response, in which case $\dot{\varepsilon} \gg 1$, and $\overline{t}_c$ is small. Equation (22) reduces to

$$[\exp(\overline{t}_c) - \overline{t}_c - 1] = \frac{\overline{t}_c^2}{2} + O(\overline{t}_c^3) = \frac{1}{\overline{\dot{\varepsilon}}} \tag{23}$$

which results in

$$\overline{t}_c = \left(\frac{2}{\overline{\dot{\varepsilon}}}\right)^{1/2} \tag{24}$$

Thus the normalized time for complete decohesion is inversely proportional to the square root of the external strain rate for very high strain rates. In dimensional form this may be written as

$$t_c = \left(\frac{\delta_c}{c\dot{\varepsilon}}\right)^{1/2} \tag{25}$$

This time scale is of practical importance. In order to properly resolve the unloading part of the cohesive law in a dynamic fragmentation simulation, the integration time step must be roughly an order of magnitude smaller. We will come back to this point in view of numerical results.

### *2.4. Illustration of cohesive element approach: crack branching simulations in PMMA*

Before discussing the topic of convergence, we illustrate the cohesive element approach with results of dynamic crack propagation and branching in PMMA. Crack branching tests are increasingly becoming a benchmark test and a number of recent papers have used it for validation purposes [21, 24, 35, 37, 38]. Here, the simulations of Falk *et al.* [24] were reproduced to test the ability of the initially rigid cohesive elements to capture crack branching in a 2D setting. Previously, we obtained probing crack branching results in 3D PMMA plates [21]. Nonetheless, it had been observed that the type of cohesive law used in this paper, might fail to capture branching mechanisms [24].



DOI: 10.1002/nme

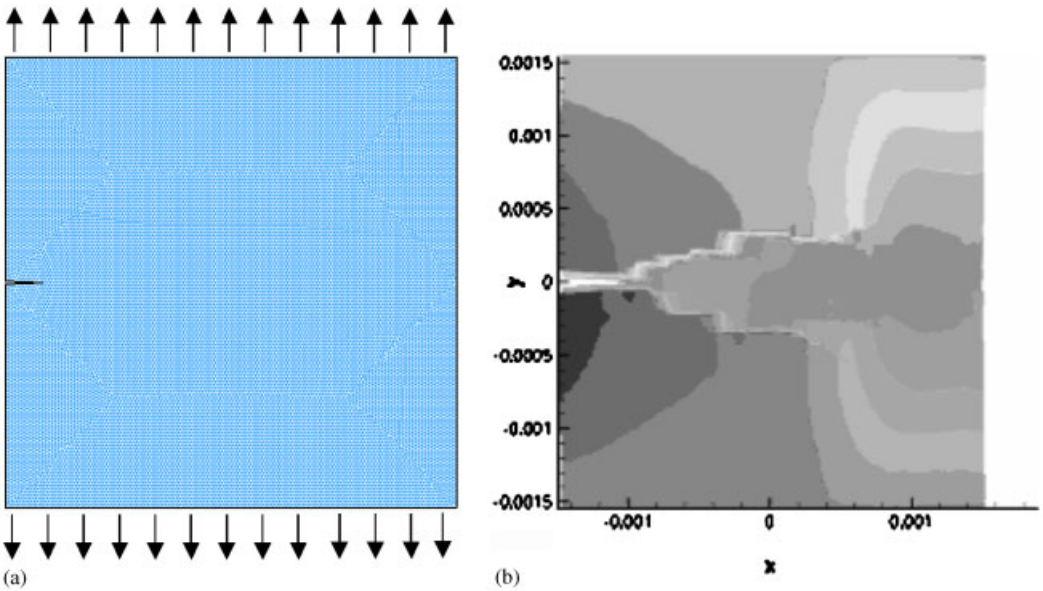


Figure 2. (a) Finite-element mesh o a PMMA plate under mode I opening (the mesh contains 36 096 T6 elements); and (b) simulation results showing crack branching, which were obtained for $W_0/G_c = 13.5$ (vertical displacement contours are shown; displacements on top and bottom boundaries are $\pm 43$ μm).

In order to test the approach in 2D as well, we have developed a 2D dynamic insertion scheme for cohesive elements. Similar to Falk *et al.* [24] we meshed a $h = 3$ mm square block of PMMA with an edge crack extending 0.25 mm into the block from the left edge. The elastic properties for PMMA are chosen to be $E = 3.24$ GPa, $\nu = 0.35$, and $\rho = 1.19$ g/cm$^3$, while the fracture properties are $G_c = 300$ N/m, and $\sigma_c = 130$ MPa. Finite-element meshes were obtained for five different mesh sizes $h_e = 64$, 48, 40, 32, and 12 μm, corresponding to a total number of nodes of 10 211, 18 201, 26 217, 41 029, and 72 713. Figure 2(a) represents the finest mesh (72 713 nodes, 36 096 elements). The cohesive zone length estimate obtained with Equation (14) is 58.5 μm. Since the cohesive zone size is bigger than all but the coarsest mesh size used in this study, we expect to be able to resolve the important details of the dynamic crack propagation process.

Different loading conditions were tested including the ones chosen in Reference [24] and in Reference [37]. In both cases, the loading is applied uniaxially by prescribing a displacement in the vertical direction on the top and bottom boundaries (the side boundaries are stress free). In Reference [24], the displacement is applied dynamically, starting from uniformly applied velocity gradients in $x$ and $y$ directions, and thereafter maintaining a constant strain rate in $y$ direction on the top and bottom boundary. This form of loading does not generate waves propagating in from the boundaries but creates a constant source of energy input in the propagating crack tip. While branching results were obtained for all meshes with this form of loading, we preferred the boundary conditions detailed in Reference [37]. There, we prescribe a fixed vertical displacement, $\delta_0$, on the top and bottom boundary and solve for the static problem. The strain energy per unit



DOI: 10.1002/nme

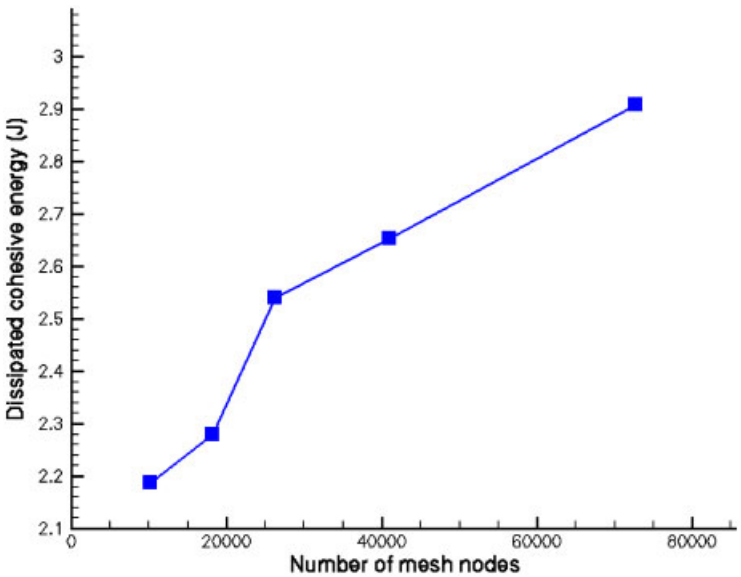


Figure 3. Cohesive energy dependence on mesh size for crack branching simulations in PMMA plate for $W_0/G_c = 13.5$.

length in a plate without a crack under fixed-grip boundary loading is well defined:

$$W_0 = \frac{2E\delta_0^2}{h} \tag{26}$$

$W_0$ becomes available for creating new surfaces when the simulation begins (experimentally this would be equivalent to introducing a sharp crack with a razor blade in a pre-strained plate [39]). Naturally, $W_0$ is a direct function of the applied displacement field. The larger the displacement the more energy is available for propagating the crack. At sufficiently high energy levels, crack branching is observed, Figure 2(b) (obtained for $W_0/G_c = 13.5$).

While the observation of consistent crack branching in successive simulations is an indication of the method's robustness, the detailed picture of energy dissipation is puzzling. All simulations that exhibited branching showed an increase in the amount of total cohesive energy dissipated as the mesh size decreased. This additional energy dissipation lead to decreasing crack velocity branching transitions, although as noted in Reference [37] they were consistently higher than experimentally observed values. Figure 3 shows energy dissipation results for the case when the ratio of strain energy stored in the plate relative to that in the cohesive zone is $W_0/G_c = 13.5$. A detailed examination of the cracked surfaces showed an increasing amount of microcracking and crack path variation as the number of nodes in the simulations increases. This trend has been observed, albeit for a different boundary value problem, by Ruiz *et al.* [17]. Could it be that energy convergence may never be attained? If numerical convergence is not an elusive goal, what mesh size should be chosen so that the amount of microcracking becomes essentially mesh independent? All meshes but one in Figure 3 resolve the cohesize zone length scale. The lack of energy convergence indicates that perhaps another criterion is needed for dynamic fracture or



DOI: 10.1002/nme

fragmentation simulations. These questions will be addressed in the next section for an idealized 1D setting.

## 3. DYNAMIC FRAGMENTATION OF A CERAMIC RING

### *3.1. Model description*

In order to simplify the problem, we strip down the simulation capability and the related complex fragmentation mechanisms to the most elementary model. Our model consists of an expanding ring, Figure 4, which has been discussed in earlier work [23, 40], and was shown to be equivalent to the fragmentation of a 1D bar under uniform tension [41]. As in Section 2.4, the material is assumed to be linearly elastic and upon reaching a critical stress, 1D initially rigid cohesive elements are inserted to monitor multiple cracks nucleation and interaction. These mechanisms depend heavily on the mechanical properties of the material and external loading. As a crack grows, unloading stress waves are emitted and relieve the neighbouring regions. The stress in an unloaded region decreases with time so that no more cracks are initiated, although an existing crack may continue to grow. If the unloading regions overlap, some nucleated cracks may begin to close. We assume that stress waves pass through closed cracks.

The 1D setting is convenient for two reasons. First, it allows the use of the method of characteristics to track stress wave interactions in the elastic material [40, 42]. Exact analytical solutions exist for capturing wave interactions. Thus, the numerical part of the method concentrates fully on the non-linear behaviour of cohesive elements, which is the focus of this paper. Nonetheless,

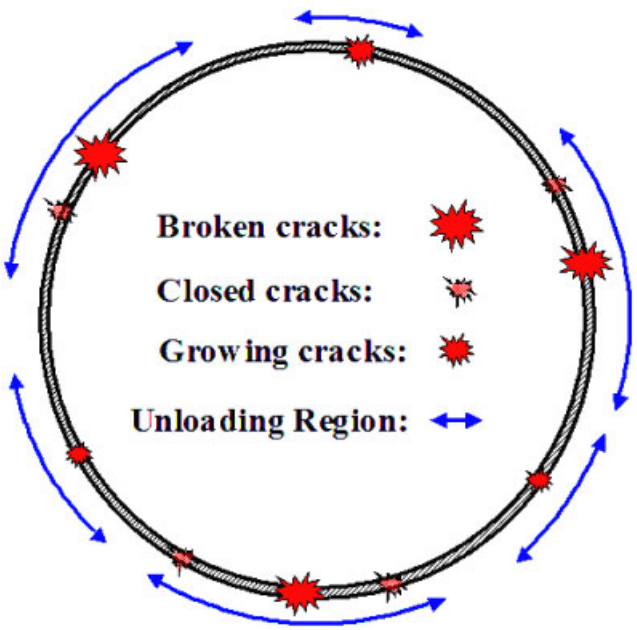


Figure 4. Schematic of a ring fragmenting under explosive loading.



DOI: 10.1002/nme

the results were also compared to finite-element calculations and no significant differences were observed. Second, the restriction of the problem to a 1D setting permits the resolution of very high mesh densities at an affordable cost. We are then able to assess unambiguously if convergence can be attained in the context of the cohesive element approach.

Our model ceramic ring has a radius ($R_0$) 7.96 mm (the circumference of the ring, $L_0 = 2\pi R_0$, is 50 mm). It is made of a material (similar to a sintered silicon nitride) with density $2.75 \times 10^3 \text{kg/m}^3$, elastic modulus 275 GPa, fracture strength ($\sigma_c$) 300 MPa and fracture energy ($G_c$) 100 N/m. A 1% random variation around $\sigma_c$ is applied at all nodes to help localize the process of fragmentation. The ring is loaded explosively with different radial speeds ($v_r$). The equivalent strain rate $\dot{\varepsilon}$ is $\dot{\varepsilon} = v_r / R_0$. Each ring fragments through the process described earlier, and fragment statistics are collected when all the fragments are formed.

### 3.2. *Numerical results*

In previous work we have described the dependence of fragment size on loading rate [23, 40]. Here we focus our attention on the numerical convergence of the solution and mostly leave aside physical discussions.

Fragmentation simulations have been conducted for 13 uniform mesh densities with number of nodes ranging from 128 to $10^6$. All these meshes have been loaded at seven different strain rates ranging from $5 \times 10^3$ to $5 \times 10^5$ $\text{s}^{-1}$. Figure 5(a) represents the energy dissipated in the process of cohesive fracture. This includes cohesive elements that have been fully damaged as well as those that are only partially damaged. For all strain rates considered we observe a

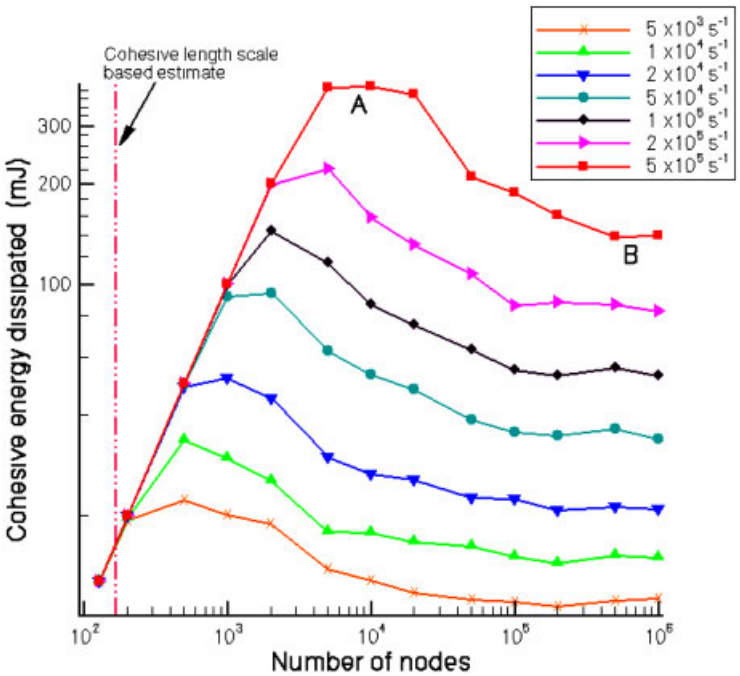


Figure 5. Cohesive energy dependence on mesh size for ring fragmentation problem.



DOI: 10.1002/nme

non-monotonic convergence. For clarity, we describe the results corresponding to the highest strain rate, e.g. $5 \times 10^5$ s$^{-1}$. All other strain rates follow a similar behaviour, although convergence is attained earlier and the magnitudes of energy dissipation are lower due to lesser amounts of microcracking.

For a strain rate of $5 \times 10^5$ s$^{-1}$ (square symbols in Figure 5(a)), we see that for coarse meshes the energy dissipated is proportional to the number of nodes in the mesh. This trend is observed roughly up to a mesh with $5 \times 10^3$ nodes. This strong mesh dependence indicates that these mesh sizes under resolve the fragmentation process. In fact, the constant slope in Figure 5(a) implies that all cohesive elements end up fully broken and thus the fragment size depends directly on the mesh size. Although Equation (14) is not directly applicable to a 1D problem we used it to get an estimate of the cohesive zone size for the material properties under consideration. The vertical line in Figure 5(a) represents the cohesive length scale based estimate. It indicates that meshes finer than 165 nodes in the 1D direction should be able to capture the cohesive zone length scale. Clearly, for this highly dynamic problem, this mesh size estimate is not satisfying, as it cannot resolve the fragmentation problem. In light of this, there may be a need for alternate cohesive zone estimates that would include a direct dependence on strain rate. We also note that the dissipated energy increases up to $10^4$ nodes (mesh A in Figure 5). Although $10^4$ nodes is a relatively small mesh in a 1D setting, its 2D equivalent is $10^8$ nodes (and $10^{12}$ nodes in 3D). Many published results using the cohesive element approach in a multidimensional space have been obtained with smaller meshes. We speculate that observations of energy increase with increasing number of nodes in the literature are due to microcracking being not properly resolved, although the increase may not be linearly proportional to the node number as boundary conditions may deviate from the simple uniaxial state of stress studied here. A relevant example is the crack branching simulations in PMMA of this paper (Figure 3).

A significant finding of this paper is that for sufficiently large meshes one can properly resolve microcracking. Indeed, for $10^4$ nodes (point A in Figure 5) a maximum in energy dissipation is attained and beyond that point a smooth convergence is observed. For large meshes ($10^6$ nodes, point B) roughly 1000 fragments are obtained (96, 125, 159, 254, 371, 580, 1000, for all seven strain rates in increasing order). This finding is very encouraging as it indicates that although cohesive elements are inserted at many more nodes than necessary most are not severely damaged and do not impact significantly the energy balance of the problem. Despite this very positive outcome for cohesive approaches, it is disturbing to notice that the same convergence may not be observed for meshes much smaller than $10^6 \times 10^6 = 10^{12}$ nodes in 2D and $10^{18}$ nodes in 3D, which are meshes beyond any available computational power.

The fact that convergence is non-monotonic deserves comments as well. One may wonder why a coarse mesh (mesh A) leads to more cohesive cracking than a much finer mesh (mesh B). After all, many more cohesive elements are present in mesh B and these may exhibit more microcracking. Our initial attempt at explaining this trend consisted in checking if the large time step corresponding to the relatively coarse mesh A was too big to unload sufficiently slowly cohesive elements (Equation (25)). However, reducing the time step by an order of magnitude did not change the results. The problem is not numerical but lies deep into the physics of fragmentation and more precisely in the inherent randomness associated with generating fragments. Figure 6 represents fragments size distributions obtained for a ceramic material at various strain rates [41]. We have shown that a simple universal law (Weibull distribution) captures fragment sizes for all strain rates [42]. The details of this law are beyond the scope of this paper but the fact that large and small fragments exist at the outcome of a fragmentation event is not. Figures 7(a) and (b) show



DOI: 10.1002/nme

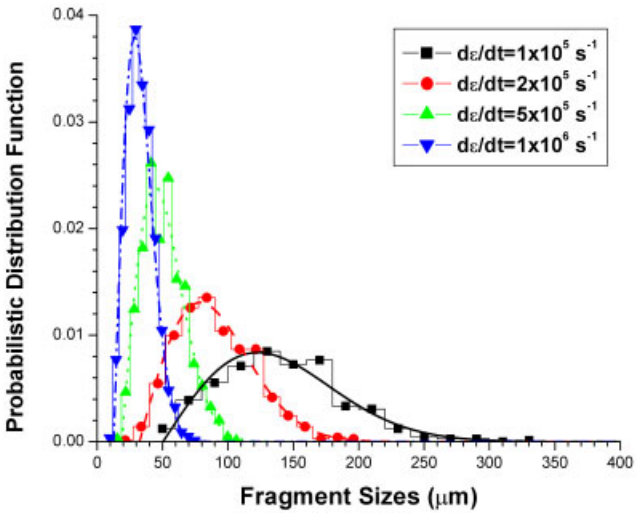


Figure 6. PDF of fragment size for a ceramic ring under different strain rates [41].

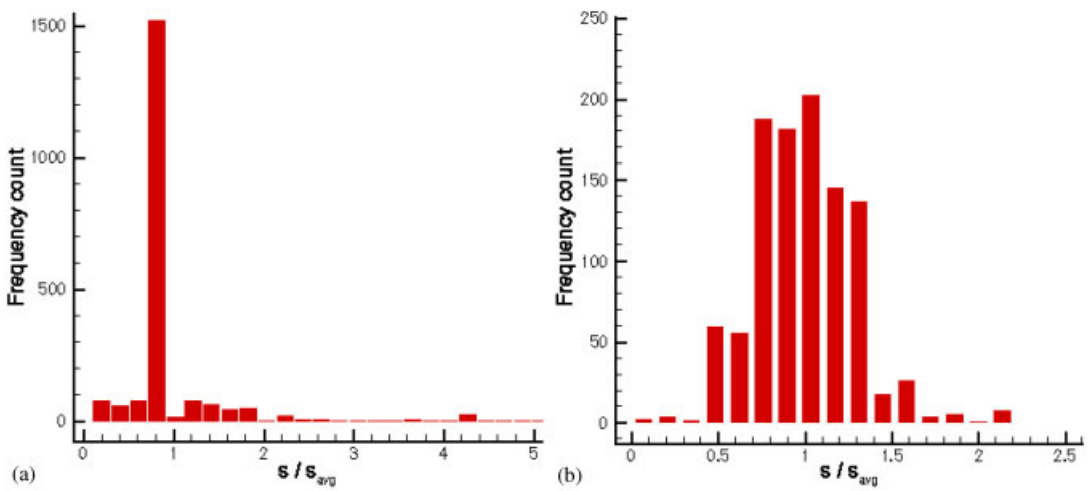


Figure 7. Fragment size distribution corresponding to: (a) mesh A; and (b) mesh B.

the fragment size distributions obtained for mesh A and mesh B, respectively. The uniformity in mesh A does not permit capturing the randomness of fragmentation. Even though the number of nodes is relatively high most fragments vary little in sizes. The highly constrained fragmentation event ultimately yields a larger number of fragments (and therefore a higher dissipated energy). Although mesh B is still uniform, the number of nodes is now sufficiently large to obtain a physical distribution of fragment sizes, Figure 7(b).

Uniform meshes severely constrain the fragmentation event and its desire to randomize fragment sizes. This explains the non-monotonic convergence observed in Figure 5. A natural question then



DOI: 10.1002/nme

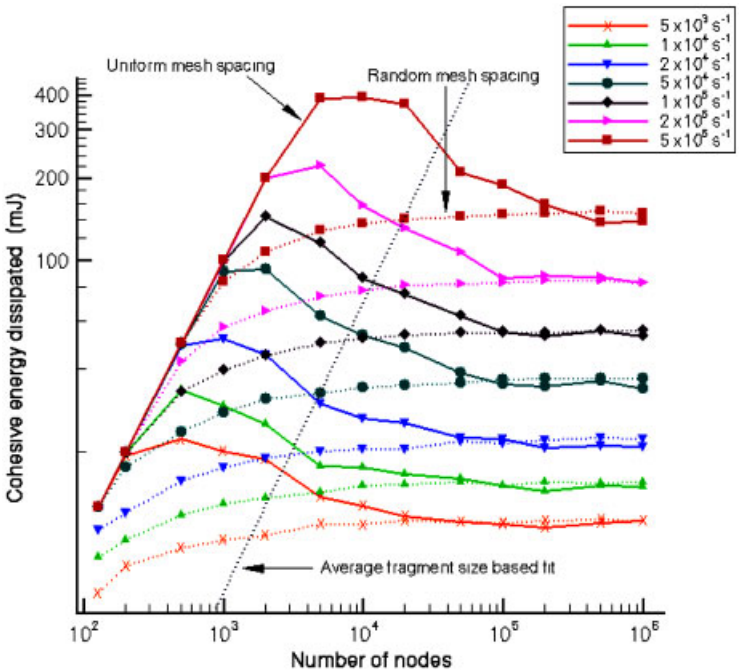


Figure 8. Effect of random mesh spacing on cohesive energy convergence. The dashed line shows the proposed fragment-size-based estimate; right of this line convergence is attained.

arises. Could random meshes lead to a different convergence pattern? The answer is yes and this in a dramatic way. The dotted lines in Figure 8 represent the results obtained for random meshes obtained by shifting each node by a random amount in between $\pm 0.4h_e$, where $h_e$ is the mesh size in the corresponding uniform mesh. For this imposed degree of randomness, we obtained a distribution of mesh sizes with the smallest and largest elements being around $0.2h_e$ and $1.8h_e$. The convergence is now monotonic and, remarkably, it is up to two orders of magnitudes faster. For a strain rate of $5 \times 10^5$ s$^{-1}$, meshes with more than $10^4$ nodes seem to capture mostly the fragmentation event (Figure 9). This relatively small number of nodes allows the extension of the analysis to higher dimension problems. For instance, parallel fragmentation simulations of 50 mm $\times$ 50 mm ceramic plates under biaxial loading, for which $10^8$ nodes may suffice, are within sight. It is also noteworthy that the smoothness of the fragment size distribution obtained for a mesh with $10^6$ nodes, Figure 9, is remarkably improved compared to those from uniform meshes, Figure 7(b). Numerical modelling of fragmentation has thus an odd characteristic: uniform meshes should be avoided at all cost.

Surprisingly, only a slight degree of mesh randomness is necessary for improving numerical solution convergence. Table I lists the energy dissipated and number of fragments obtained by imposing varying degrees of mesh heterogeneity. Random displacements of nodes by an amount in between $\pm 0.05h_e$ suffice to improve convergence by roughly two orders of magnitude. It is however possible that an optimum mesh size distribution may be found to achieve fastest convergence. There, fragmentation analytical studies based on the principle of maximum entropy [43–45] may prove useful to determine the mesh density functional.



DOI: 10.1002/nme

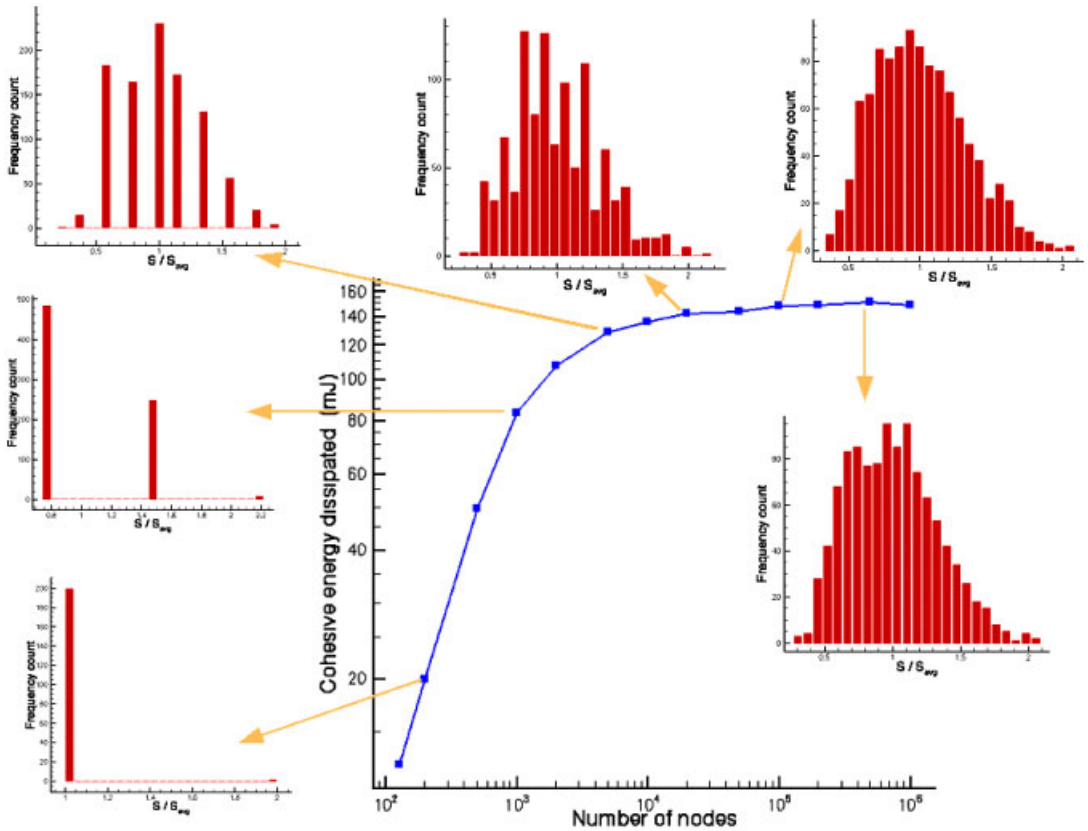


Figure 9. Mesh dependence of fragment size distribution (random mesh spacing) for $5 \times 10^5$ $s^{-1}$ strain rate.

Table I. Effect of different perturbation factors on energy dissipated and number of fragments (for $5 \times 10^5$ $s^{-1}$).

| Perturbation factor (as % of $h_e$) | Energy dissipated (mJ) | # fragments |
|---|---|---|
| 0 | 393.4 | 2723 |
| 5 | 152.1 | 1093 |
| 10 | 147.2 | 1065 |
| 15 | 143.8 | 1042 |
| 20 | 142.0 | 1047 |
| 25 | 139.7 | 1038 |
| 30 | 136.2 | 1015 |
| 35 | 136.4 | 1018 |
| 40 | 134.7 | 994 |



DOI: 10.1002/nme

As discussed earlier, at least in a 1D setup, cohesive zone estimates such as Equation (14), lead to meshes too coarse to capture all microcracking events. It is therefore of interest to establish an alternate estimate, even if empirical. A key finding of our previous work [42] was that a universal law may be used to capture the dependence of the average fragment size with strain rate. This estimate was proposed as an alternate to Grady's energy-based model [46], which does not take into account dynamical effects. The proposed equation, which captures accurately a wide range of ceramic materials, is

$$\frac{s}{s_0} = 4.5\left[1 + 4.5\left(\frac{\dot{\varepsilon}}{\dot{\varepsilon}_0}\right)^{2/3}\right]^{-1} \tag{27}$$

where $s$ is the average fragment size, $\dot{\varepsilon}$ is the strain rate, $\dot{\varepsilon}_0 = (\sigma_c/E)/t_0$ is the characteristic strain rate (Equation (18) [36]), and $s_0 \equiv ct_0$ is the characteristic fragment size. These latter parameters both depend on the characteristic time $t_0 = \rho c \delta_c / 2\sigma_c$ (Equation (13)).

Many fragments end up being smaller than the average fragment size. In a 1D setting, a mesh size that is roughly one order of magnitude smaller than the average size leads to converged results. Our mesh size estimate, expanded to explicitly present all the material parameters, is

$$h_e = 0.25(EG_c/\sigma_c^2)\left[1 + 4.5\left(\frac{\dot{\varepsilon}}{c\sigma_c^3/E^2G_c}\right)^{2/3}\right]^{-1} \tag{28}$$

The number of nodes corresponding to Equation (28) is shown by the dashed line in Figure 8. It seems to be a reasonable indicator of the occurrence of convergence for the range of strain rates studied. Other estimates, perhaps incorporating time scales such as Equation (25), may be proposed. Based on these estimates, converged 2D fragmentation simulations are within reach. 3D simulations, on the other hand, remain perhaps too computationally intensive to achieve fully converged solutions. There, cohesive approaches would be well served to take into account the poor resolution of microcracking events. Rate-dependent cohesive laws, for which $G_c$ becomes an increasing function of strain rate, are promising in this regard [37, 47, 48]. In addition, a worthy research direction consists in checking, for dynamic fragmentation problems, convergence properties of other numerical approaches. In this regard partition of unity methods [49] as well as discrete and meshfree methods [50, 51], may lead to faster convergence as crack locations are not constrained to appear at element boundaries. Initially, these cross comparisons could be conducted in a 1D setting.

## 4. CONCLUSIONS

The main theme of this paper has been energy convergence of the cohesive element approach for the fragmentation analysis of a linear elastic material. While the discussion has not addressed crack path convergence, substantial computational evidence demonstrates, for the first time, that the cohesive element method converges in an energetic sense, at least in a simple one-dimensional setting. Microcracking events and the ensuing fragment sizes distributions are statistically mesh independent for sufficiently fine meshes. Remarkably, convergence was attained up to two orders of magnitude earlier for random meshes than for uniform meshes, and that even for very small random perturbations. It should be emphasized that standard cohesive zone size estimates under



DOI: 10.1002/nme

resolve the number of nodes necessary for attaining mesh independence in dynamic fragmentation simulations. This may explain why energy convergence of the cohesive element approach had not been previously observed. We have proposed a simple mesh density estimate based on the dependence of the average fragment size on the strain rate and elastic and fracture material properties. This estimate provides a clear roadmap for extending the findings of this paper to more complex loading conditions including biaxial loading of ceramic plates.

## ACKNOWLEDGEMENTS

The support of the Army Research Office under the grant number 48389-MS is gratefully acknowledged as well as the support of the Army Research Laboratory through a subcontract from the University of Nebraska Lincoln under the grant number 2511050005200.

## REFERENCES

1. Piekutowski AJ. Fragmentation of a sphere initiated by hypervelocity impact with a thin sheet. *International Journal of Impact Engineering* 1995; **17**:627–638.
2. De Chant L. Validation of a computational implementation of the Grady–Kipp dynamic fragmentation theory for thin metal plate impacts using an analytical strain-rate model and hydrodynamic analogues. *Mechanics of Materials* 2005; **37**:83–94.
3. Grady DE, Kipp ME. Continuum modelling of explosive fracture in oil shale. *International Journal of Rock Mechanics and Mining Sciences* 1980; **17**:147–157.
4. Brown WK, Karp RR, Grady DE. Fragmentation of the Universe. *Journal of Astrophysics and Space Science* 1983; **94**(2):401–412.
5. Espinosa HD, Brar NS, Yuan G, Xu Y, Arrieta V. Enhanced ballistic performance of confined multi-layered ceramic targets against long rod penetrators through interface defeat. *International Journal of Solids and Structures* 2000; **37**(36):4893–4913.
6. Normandia MJ. Impact response and analysis of several silicon carbides. *International Journal of Applied Ceramic Technology* 2004; **1**(3):226–234.
7. Dugdale DS. Yielding of steel sheets containing slits. *Journal of the Mechanics and Physics of Solids* 1960; **8**:100–104.
8. Barrenblatt GI. The mathematical theory of equilibrium of cracks in brittle fracture. *Advances in Applied Mechanics* 1962; **7**:55–129.
9. Xu XP, Needleman A. Numerical simulations of fast crack growth in brittle solids. *Journal of the Mechanics and Physics of Solids* 1994; **42**:1397–1434.
10. Xu XP, Needleman A. Numerical simulations of dynamic interfacial crack growth allowing for crack growth away from the bond line. *International Journal of Fracture* 1995; **74**:253–275.
11. Xu XP, Needleman A. Numerical simulations of dynamic crack growth along an interface. *International Journal of Fracture* 1996; **74**:289–324.
12. Camacho GT, Ortiz M. Computational modelling of impact damage in brittle materials. *International Journal of Solids and Structures* 1996; **33**:2899–2938.
13. Camacho GT, Ortiz M. Adaptive Lagrangian modelling of ballistic penetration of metallic targets. *Computational Methods in Applied Mechanical Engineering* 1997; **142**:269–301.
14. Pandolfi A, Krysl P, Ortiz M. Finite element simulation of ring expansion and fragmentation: the capturing of length and time scales through cohesive models of fracture. *International Journal of Fracture* 1999; **95**:279–297.
15. Pandolfi A, Guduru PR, Ortiz M, Rosakis AJ. Three dimensional cohesive-elements of dynamic fracture in C300 steel. *International Journal of Solids and Structures* 2000; **37**:3733–3760.
16. Ruiz G, Ortiz M, Pandolfi A. Three dimensional finite-element simulation of the dynamic Brazilian tests on concrete cylinders. *International Journal for Numerical Methods in Engineering* 2000; **48**:963–994.
17. Ruiz G, Ortiz M, Pandolfi A. Three dimensional cohesive modeling of dynamic mixed-mode fracture. *International Journal for Numerical Methods in Engineering* 2001; **52**:97–120.
18. Zhai J, Zhou M. Finite element analysis of micromechanical failure modes in a heterogeneous ceramic material system. *International Journal of Fracture* 2000; **101**:161–180.



DOI: 10.1002/nme

19. Zavattieri PD, Espinosa HD. Grain level analysis of crack initiation and propagation in brittle materials. *Acta Materialia* 2001; **49**:4291–4311.
20. Zhou F, Molinari JF. Stochastic fracture of ceramics under dynamic tensile loading. *International Journal of Solids and Structures* 2004; **41**(22–23):6573–6596.
21. Zhou F, Molinari JF. Dynamic crack propagation with cohesive elements: a methodology to address mesh dependency. *International Journal for Numerical Methods in Engineering* 2004; **59**(1):1–24.
22. Maiti S, Rangaswamy K, Geubelle PH. Mesoscale analysis of dynamic fragmentation of ceramics under tension. *Acta Materialia* 2005; **53**(3):823–834.
23. Zhou F, Molinari JF, Ramesh KT. Effects of material properties on the fragmentation of brittle materials. *International Journal of Fracture* 2005, in press.
24. Falk ML, Needleman A, Rice JR. A critical evaluation of cohesive zone models of dynamic fracture. *Journal de Physique IV*, *Proceedings* 2001; 5.43–5.50.
25. Rice JR. Some studies of crack dynamics. In *Physical Aspects of Fracture*; *Proceedings of NATO Advanced Study Institute on Physical Aspects of Fracture*, 5–17, Cargese, Corsica, June 2000.
26. Papoulia KD, Vavasis S, Ganguly P. Spatial convergence of crack nucleation using a cohesive finite element model on a pinwheel-based mesh. *International Journal for Numerical Methods in Engineering* 2006, in press.
27. Hughes TLJ. *The Finite Element Method*: *Linear Static and Dynamic Finite Element Analysis*. Prentice-Hall: Englewood Cliffs, NJ, 1987.
28. Pandolfi A, Ortiz M. An efficient adaptive procedure for three-dimensional fragmentation simulations. *Engineering with Computers* 2002; **18**:148–159.
29. Papoulia KD, Sam CH, Vavasis SA. Time continuity in cohesive finite element modeling. *International Journal for Numerical Methods in Engineering* 2003; **58**(5):679–701.
30. Rice JR. Mathematical analysis in the mechanics of fracture. In *Fracture*, *An Advanced Treatise*, *Vol. II*: *Mathematical Fundamentals*, Liebowitz H (ed.). Academic Press: New York, 1968; 191–311.
31. Schapery RA. A theory of crack initiation and growth in viscoelastic media. *International Journal of Fracture* 1975; **11**(1):141–159.
32. Rice JR. The mechanics of earthquake rupture. In *Physics of the Earth's Interior* (*Proceedings of International School of Physics* 'Enrico Fermi'), Dziewonski AM, Boschi E (eds). North-Holland: Amsterdam, 1980; 555–649.
33. Williams ML. On the stress distribution at the base of a stationary crack. *Journal of Applied Mechanics* 1957; **24**:109–114.
34. Palmer AC, Rice JR. The growth of slip surfaces in the progressive failure of over-consolidated clay. *Proceedings of the Royal Society of London*, *Series A* 1973; **332**:527–548.
35. Yu C, Pandolfi A, Ortiz M, Coker D, Rosakis AJ. Three-dimensional modeling of intersonic shear-crack growth in asymmetrically loaded unidirectional composite plates. *International Journal of Solids and Structures* 2002; **39**(25):6135–6157.
36. Drugan WJ. Dynamic fragmentation of brittle materials: analytical mechanics-based models. *Journal of the Mechanics and Physics of Solids* 2001; **49**:1181–1208.
37. Zhou F, Molinari JF, Shioya T. A rate-dependent cohesive model for simulating dynamic crack propagation in brittle materials. *Engineering Fracture Mechanics* 2005; **72**:1383–1410.
38. Areias PMA, Belytschko T. Analysis of three-dimensional crack initiation and propagation using the extended finite element method. *International Journal for Numerical Methods in Engineering* 2005; **63**(5):760–788.
39. Shioya T, Zhou F. Dynamic fracture toughness and crack propagation in brittle material. *Proceedings of IUTAM Symposium on Constitutive Relation in High/Very High Strain Rates*, Noda, Japan, 1995; 105–112.
40. Zhou F, Molinari JF, Ramesh KT. A cohesive model based fragmentation analysis: effects of strain rate and initial defect distribution. *International Journal of Solids and Structures* 2005; **42**(18–19):5181–5207.
41. Zhou F, Molinari JF, Ramesh KT. A finite difference analysis of the brittle fragmentation of an expanding ring. *Computational Materials Science* 2005, in press.
42. Zhou F, Molinari JF, Ramesh KT. Characteristic fragment size distribution of dynamically expanding rings. *Applied Physics Letters* 2005, submitted.
43. Englman R, Rivier N, Jaeger Z. Size-distribution in sudden breakage by the use of entropy maximization. *Journal of Applied Physics* 1988; **63**(9):4766–4768.
44. Raz T, Even U, Levine RD. Fragment size distribution in cluster impact: shattering versus evaporation by a statistical approach. *Journal of Chemical Physics* 1995; **103**(13):5394–5409.
45. Smalley LL, Woosley JK. Application of steady state maximum entropy methods to high energy impacts on ceramic targets. *International Journal of Impact Engineering* 1999; **23**:869–882.



DOI: 10.1002/nme

46. Grady DE. Local inertial effects in dynamic fragmentation. *Journal of Applied Physics* 1982; **53**(1):322–325.
47. Bazant ZP, Li Y-N. Cohesive crack with rate-dependent opening and viscoelasticity: 1. Mathematical model and scaling. *International Journal of Fracture* 1997; **86**:247–265.
48. Li Y-N, Bazant ZP. Cohesive crack with rate-dependent opening and viscoelasticity: 2. Numerical algorithm, behavior and size effect. *International Journal of Fracture* 1997; **86**:267–288.
49. Moes N, Dolbow J, Belytschko T. A finite element method for crack growth without remeshing. *International Journal for Numerical Methods in Engineering* 1999; **46**(1):131–150.
50. Belytschko T, Chen H, Xu JX, Zi G. Dynamic crack propagation based on loss of hyperbolicity and a new discontinuous enrichment. *International Journal for Numerical Methods in Engineering* 2003; **58**(12):1873–1905.
51. Rabczuk T, Belytschko T. Cracking particles: a simplified meshfree method for arbitrary evolving cracks. *International Journal for Numerical Methods in Engineering* 2004; **61**(13):2316–2343.



DOI: 10.1002/nme